

# Non-thermal photons and $\text{H}_2$ formation in the early Universe

C. M. Coppola<sup>1,2,3</sup>  $\star$ , D. Galli<sup>3</sup>, F. Palla<sup>3</sup>, S. Longo<sup>2,3,4</sup>, J. Chluba<sup>5</sup>

<sup>1</sup>*Department of Physics and Astronomy, University College London, Gower Street, London WC1E 6BT*

<sup>2</sup>*Università degli Studi di Bari, Dipartimento di Chimica, Via Orabona 4, I-70126, Bari, Italy*

<sup>3</sup>*INAF-Osservatorio Astrofisico di Arcetri, Largo E. Fermi 5, I-50125 Firenze, Italy*

<sup>4</sup>*IMIP-CNR, Section of Bari, via Amendola 122/D, I-70126 Bari, Italy*

<sup>5</sup>*Johns Hopkins University, Bloomberg Center 435, 3400 N. Charles St., Baltimore, MD 21218*

Accepted 2013 June 5. Received 2013 June 5; in original form 2013 April 22

## ABSTRACT

The cosmological recombination of H and He at  $z \simeq 10^3$  and the formation of  $\text{H}_2$  during the dark ages produce a non-thermal photon excess in the Wien tail of the cosmic microwave background (CMB) blackbody spectrum. Here we compute the effect of these photons on the  $\text{H}^-$  photodetachment and  $\text{H}_2^+$  photodissociation processes. We discuss the implications for the chemical evolution of the Universe in the post-recombination epoch, emphasizing how important a detailed account of the full vibrational manifold of  $\text{H}_2$  and  $\text{H}_2^+$  in the chemical network is. We find that the final abundances of  $\text{H}_2$ ,  $\text{H}_2^+$ ,  $\text{H}_3^+$  and HD are significantly smaller than in previous calculations that neglected the effect of non-thermal photons. The suppression is mainly caused by extra hydrogen recombination photons and could affect the formation rate of first stars. We provide simple analytical approximations for the relevant rate coefficients and briefly discuss the additional effect of dark matter annihilation on the considered reaction rates.

**Key words:** molecular processes; cosmology: early Universe.

## 1 INTRODUCTION

In the era of precision cosmology, the determination of the chemical composition of the early Universe requires an accurate evaluation of the reaction rates of the main chemical processes involved. A detailed chemical-kinetic model for the evolution of the homogeneously expanding Universe in the post-recombination epoch is also needed to follow the collapse of primordial clouds and hence to study the formation of the first-generation stars (Tegmark et al. 1997; Abel et al. 2002; Bromm et al. 2002). In particular,  $\text{H}_2$  represents a “key” element because of its abundance and coolant properties. For this reason the line emissions associated with molecular hydrogen could in principle give informations about the matter distribution during the phase of pre-reionization of the Universe (e.g., Ciardi & Ferrara 2001; Gong et al. 2012). Over the past years continuous improvements have been made to the modeling of the early

Universe chemistry under non-equilibrium conditions. For example, Coppola et al. (2011, hereafter C11), Longo et al. (2011) and Coppola et al. (2012) demonstrated the importance of taking into account the complete internal states of chemical partners in a chemical network for the primordial gas, as well as all non-equilibrium processes occurring at high redshift  $z$ .

In this paper we compute the abundance of the main chemical species (such as  $\text{H}_2$ ,  $\text{H}_2^+$ ,  $\text{H}^-$ , HD and  $\text{H}_3^+$ ), including the effect of non-thermal photons due to cosmological recombination of H and He (see Sunyaev & Chluba 2009, for overview), and the radiative cascade following the formation of  $\text{H}_2$ . The non-thermal photons appear as an excess in the Wien tail of the CMB blackbody spectrum and thus significantly affect the  $\text{H}^-$  photodetachment and  $\text{H}_2^+$  photodissociation processes during the dark ages. As we show here, the main effect is caused by the extra HI recombination photons released at  $z \lesssim 100$ , limiting the formation of  $\text{H}_2$ ,  $\text{H}_2^+$ ,  $\text{H}_3^+$  and HD. We also estimate the effect of extra ionizations from annihilating dark matter particles on the  $\text{H}^-$  photodetachment rate, finding a sensitivity of the early Universe chemistry to this process (see Appendix B).

$\star$  e-mail: carla.coppola@chimica.uniba.it; galli@arcetri.astro.it; palla@arcetri.astro.it; savino.longo@ba.imip.cnr.it; jchluba@pha.jhu.edu

The paper is organized as follows: in Sections 2-3 we describe the computational methods, providing expressions for the spectral distortion of the CMB introduced by emission processes occurring in past epochs of the expanding Universe. The distortion spectra resulting from primordial atomic recombination and non-equilibrium  $\text{H}_2$  radiative cascade are then used to evaluate non-thermal reaction rates for photo-processes involving the main ‘‘catalytic’’ species for  $\text{H}_2$  formation ( $\text{H}_2^+$  and  $\text{H}^-$ ). In Section 3, we describe the time-dependent kinetics and summarize the reaction rates and cosmological parameters introduced. The resulting fractional abundances of several atomic and molecular species adopting the updated rate coefficients of Coppola et al. (2011) are discussed in Section 4.

## 2 EFFECT OF NON-THERMAL PHOTONS

Every radiative transition from an upper atomic level  $i$  to a lower level  $j$  is associated with the emission of a photon, causing a spectral distortion  $I_{ij}(\nu)$ . Assuming a very narrow emission-profile, the observing frequency  $\nu$  at some redshift  $z < z_{\text{em}}$ , is related to the rest frame frequency,  $\nu_{ij}$ , of the transition  $i \rightarrow j$  by  $\nu = \nu_{ij}(1+z)/(1+z_{\text{em}})$ . For this reason, the redshift at which the transition happens is labelled as  $z_{\text{em}}$ . The spectral distortion produced by the emission process at  $z_{\text{em}}$  and observed at redshift  $z < z_{\text{em}}$  can be written as (e.g., see Rubiño-Martin et al. 2006):

$$I_{ij}^z(\nu) = \left( \frac{hc}{4\pi} \right) \frac{\Delta R_{ij}(z_{\text{em}})(1+z)^3}{H(z_{\text{em}})(1+z_{\text{em}})^3} \quad (1)$$

where  $H(z) = H_0[\Omega_r(1+z)^4 + \Omega_m(1+z)^3 + \Omega_k(1+z)^2 + \Omega_\Lambda]^{1/2}$  is the Hubble function and  $\Delta R_{ij}$  is related to the level populations,  $N_i$  and  $N_j$  of the  $i^{\text{th}}$  and  $j^{\text{th}}$  levels by:

$$\Delta R_{ij} = p_{ij} A_{ij} N_i \frac{e^{h\nu_{ij}/k_B T_r}}{e^{h\nu_{ij}/k_B T_r} - 1} \left[ 1 - \frac{g_i N_j}{g_j N_i} e^{-h\nu_{ij}/k_B T_r} \right], \quad (2)$$

where  $p_{ij}$  is the Sobolev-escape probability,  $g_i$  and  $g_j$  the degeneracy of upper and lower levels, respectively (both factors are equal to one in the case of transitions occurring among the vibrational manifold),  $A_{ij}$  is the Einstein coefficient of the transition and  $T_r = 2.726(1+z_{\text{em}})$  K (Fixsen et al. 1996; Fixsen 2009).

To evaluate the contribution of spectral distortions to the reaction rate of a photo-reaction at a given redshift  $z$ , the integration over the actual photon distribution should be carried out:

$$k_{\text{ph}}(z) = 4\pi \int_0^\infty \frac{\sigma(\nu)}{h\nu} \left[ B_z(\nu) + \sum_{i \rightarrow j} I_{ij}^z(\nu) \right] d\nu. \quad (3)$$

Here  $\sigma(\nu)$  is the cross section of the photo-reaction as a function of frequency,  $B_z(\nu)$  the Planck distribution at  $T_r$  corresponding to the redshift  $z$  at which the reaction rate is calculated, and  $I_{ij}^z(\nu)$  the spectral distortion.

Several physical and chemical processes can modify the pure blackbody shape of the CMB (see Chluba & Sunyaev 2012, for some example related to early energy release); in the present calculations, we consider the primordial recombination of H and He and the non-equilibrium radiative cascade of  $\text{H}_2$  as sources of distortion photons. For the former,

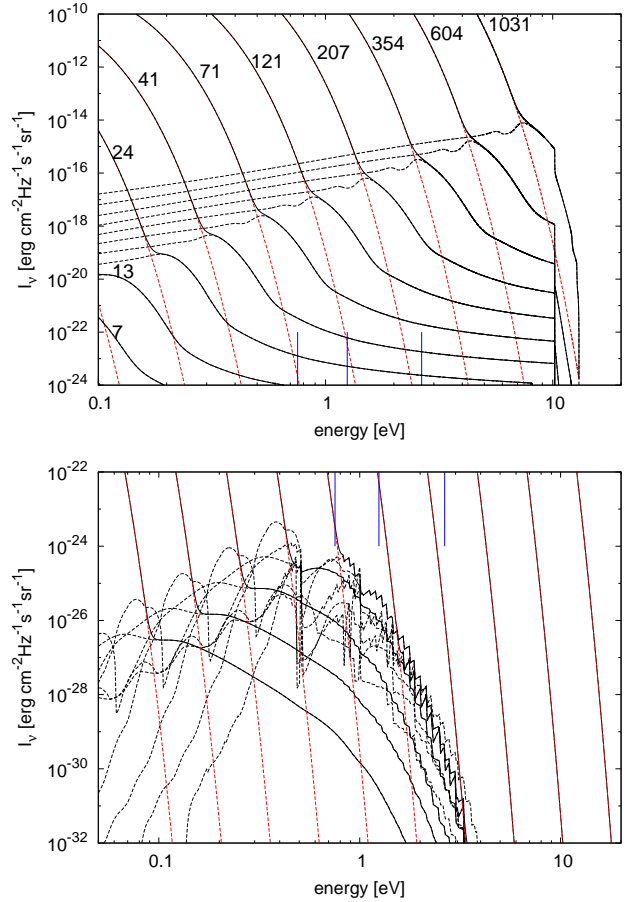


**Figure 1.** Photons spectra at several  $z$ , corresponding to the values shown in the figure (dashed lines: partial contributions; red and black lines: CMB and distortions, respectively; solid lines: total spectra). *Top panel:* blackbody and distortion photons produced by the cosmological recombination of H; *bottom panel:* blackbody plus photons produced by the radiative cascade following the non-equilibrium formation of  $\text{H}_2$  at the same redshifts. The vertical blue lines represent the thresholds for the processes considered in the present work: from the lowest energy, the threshold for  $\text{H}^-$  photodetachment (0.754 eV),  $\text{H}_2^+(v=0)$  and  $\text{H}_2^+(v=6)$  photodissociation (2.65 eV and 1.247 eV, respectively). The value for the highest vibrational level,  $\text{H}_2^+(18)$ , is 0.0029 eV, out of the range of the present figure.

the outputs of COSMORREC<sup>1</sup> (Chluba & Thomas 2011) are used to evaluate the non-thermal photon contribution. For the latter, the values of  $A_{ij}$  were calculated as in C11 averaging over the initial rotational levels and summing over the final ones the rovibrationally resolved Einstein coefficients computed by Wolniewicz et al. (1998); the non-equilibrium level populations calculated in C11 at several  $z$  have been used, following the treatment of Coppola et al. (2012).

To estimate the effect of non-thermal photons on the  $\text{H}_2$  chemistry, the main formation channels for molecular hydrogen, namely the  $\text{H}_2^+$  and  $\text{H}^-$  pathways, should be considered separately. Figure 1 shows the spectrum of the CMB at several redshifts, including the distortion photons pro-

<sup>1</sup> [www.chluba.de/CosmoRec](http://www.chluba.de/CosmoRec)

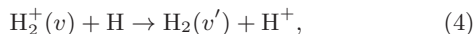
duced by the cosmological H recombination and the H<sub>2</sub> radiative cascade. For the cosmological recombination radiation, only the emission of the Ly- $\alpha$ , Ly- $\beta$  and Ly- $\gamma$  lines and the 2s-1s two-photon continuum are shown, with the computation including detailed radiative transfer effects, such as line feedback and two-photon processes. The position of the Ly- $\alpha$  line can be noticed in the upper panel of Fig. 1, while photons above  $\simeq 10.2$  eV are caused by the Ly- $\beta$  and Ly- $\gamma$  transitions. Relative to the Ly- $\alpha$  line these resonances only add a small number of photons in the far Wien tail of the CMB (Chluba & Sunyaev 2007) and thus do not affect the final results for the reaction rates at a significant level. We also omitted the emission caused by transitions among excited states (Rubiño-Martín et al. 2006; Chluba & Sunyaev 2006; Chluba, Rubiño-Martín & Sunyaev 2007), since these only give rise to a tiny derivation relative to the CMB blackbody spectrum. The reprocessing of helium photons emitted at  $z \simeq 2000$  was also taken into account for the computation of the distortion (Chluba & Sunyaev 2010), producing a pre-recombination feature in the H I Ly- $\alpha$  recombination spectrum (see also Rubiño-Martín et al. 2008).

Helium photons only directly affect the H<sub>2</sub><sup>+</sup> and H<sup>-</sup> formation rates close to  $z \simeq 2400$ , so that we did not present their contribution to the CMB spectrum separately.

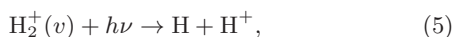
The lower panel of Fig. 1 shows the distortion produced by the radiative cascade following the non-equilibrium formation of H<sub>2</sub>. At the highest redshift, the largest contribution comes from the most energetic  $\sim 4.7$  eV transition between vibrational state  $v = 14$  and the vibrational ground level of H<sub>2</sub> molecules. At lower redshifts, the high- $v$  transitions become progressively less important because of the expansion of the Universe that shifts them to lower energies. The features present in the spectra produced by molecular radiative cascade lines reflect the presence of many transitions with  $\Delta v \geq 1$ . As a consequence, the spectra are broader than the ones obtained for the atomic recombination (Fig. 1). As for the cosmological recombination distortion, the photons produced by H<sub>2</sub> radiative transitions give rise to an excess in the far Wien tail of the CMB. The extra photons are introduced at late times, during the dark ages, when most of the H<sub>2</sub> is forming. In comparison to the recombination radiation it is, however, much smaller and thus only leads to a tiny correction to the reaction rates.

## 2.1 H<sub>2</sub><sup>+</sup> channel

Charge transfer between H<sub>2</sub><sup>+</sup> and H,



represents the dominant formation channel of H<sub>2</sub> at high  $z$ . The reaction (4) is exoergic for all vibrational states,  $v$ , unlike the charge transfer between H<sub>2</sub> and H<sup>+</sup> that is endoergic for  $v \leq 3$ , although with low threshold energies (e.g. Krstić & Schultz 1999, Krstić et al. 2002, Krstić 2002,2003,2005). For the conditions of the primordial Universe a very efficient collisional way to destroy H<sub>2</sub><sup>+</sup> is by dissociative recombination (Motapon et al. 2008; Takagi 2002). Among the photo-processes, the reaction



represents a favourable destruction pathway and it has been the subject of several theoretical quantum chemistry stud-

ies (Dunn 1968; Argyros 1974; Stancil 1994; Lebedev et al. 2000, 2003). In this work, we adopt the cross sections calculated by Mihajlov et al. (2007) using a quantum mechanical method in which the photodissociation process is assumed to be the result of radiative transitions between the ground and the first excited adiabatic electronic state of the molecular ion H<sub>2</sub><sup>+</sup>. These transitions are the results of the interaction of the electron component of the ion-atom system with the free electromagnetic field in the dipole approximation. The cross sections are given as Maxwell-Boltzmann averages (i.e., assuming statistical equilibrium populations for the  $J$ -substates) of the state-to-state resolved cross sections  $\sigma_{v,J}(\lambda)$  over the rovibrational distribution function at each temperature:

$$\begin{aligned} \sigma_{\text{ph}}(\lambda, T) = \frac{1}{Z} \sum_v \left[ \sum_{J \text{ odd}} \frac{3}{2} (2J+1) e^{-\frac{E_{v,J} - E_{0,0}}{k_B T}} \sigma_{v,J}(\lambda) \right. \\ \left. + \sum_{J \text{ even}} \frac{1}{2} (2J+1) e^{-\frac{E_{v,J} - E_{0,0}}{k_B T}} \sigma_{v,J}(\lambda) \right], \end{aligned} \quad (6)$$

where  $Z$  is the partition function,

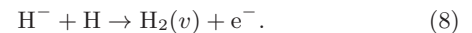
$$\begin{aligned} Z = \sum_v \left[ \sum_{J \text{ odd}} \frac{3}{2} (2J+1) e^{-\frac{E_{v,J} - E_{0,0}}{k_B T}} \right. \\ \left. + \sum_{J \text{ even}} \frac{1}{2} (2J+1) e^{-\frac{E_{v,J} - E_{0,0}}{k_B T}} \right]. \end{aligned} \quad (7)$$

The temperature used in these equations is the radiation temperature because of the conditions present in the early Universe. As a check in support of this assumption, it can be shown that for the majority of the pairs  $(v, v')$ , the critical density  $n_{cr} = A_{v,v'} / \gamma_{v,v'}$  (i.e. the ratio between radiative and collisional de-excitation coefficients) is much above the mean density of the primordial Universe. Moreover, the hypothesis of thermalization of rovibrational levels has been assumed to make calculations more feasible. This is justified considering the faster relaxation times of rotation with respect to the other molecular degrees of freedom.

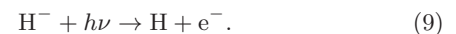
In Figure 2 we show the adopted set of average cross sections. Both the CMB blackbody and non-thermal reaction rates have been calculated using Eq. (3). The former is compared to the fit given by Galli & Palla 1998 (hereafter GP98), obtained using data by Stancil (1994) and Argyros (1974). The results shown in Figure 3 indicate that the comparison between the thermal reaction rates is satisfactory at all redshifts. At low temperatures (corresponding to  $z < 300$ ), the dominant effect is due to the non-thermal tails deriving from atomic recombination. The contribution from the H<sub>2</sub> cascade is negligible across the temperature interval.

## 2.2 H<sup>-</sup> channel

The formation of H<sub>2</sub> at low redshifts is controlled by the associative detachment process (Pagel 1959; Čížek et al. 1998; Flower 2000; Dalgarno 2005; Kreckel et al. 2010; Schlemmer 2011):



The reaction responsible for the loss of H<sup>-</sup> is the photodetachment process:



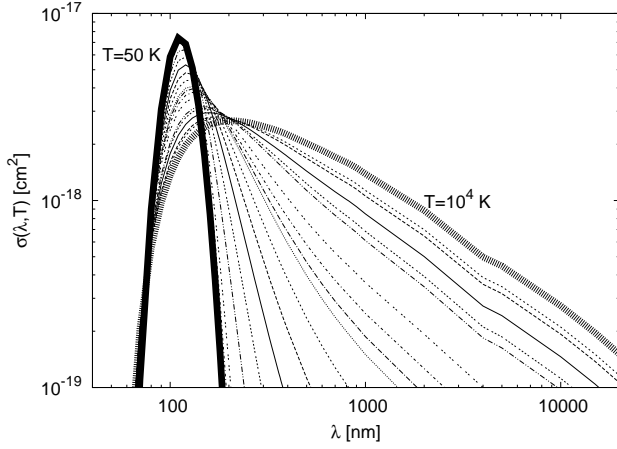


**Figure 2.**  $\text{H}_2^+$  photodissociation cross sections averaged at several temperatures, from  $T = 10^4$  K to 50 K. The intermediate curves are for  $T = 8400, 8000, 7000, 6300, 6000, 5000, 4200, 4000, 3500, 3000, 2500, 2000, 1500, 1000, 750, 500, 300, 200,$  and 100 K. Calculations have been performed by Mihajlov and Ignjatović using the theoretical method described in Mihajlov et al. 2007 on an extended temperature grid (priv. comm.)

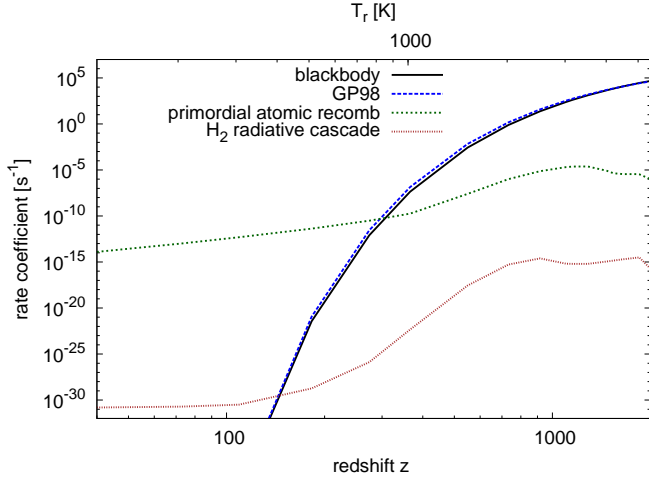


**Figure 3.**  $\text{H}_2^+$  photodissociation rate coefficient as function of redshift  $z$  (lower scale) and radiation temperature  $T_{\text{rad}}$  (upper scale). *Black solid curve:* thermal reaction rate calculated using the cross sections shown in Figure 1; *blue dashed curve:* fit by GP98. *Green dotted curve:* non-thermal contribution due to cosmological recombination photons computed with the cross sections of Figure 1. *Red small dashed curve:* same as above, with photons produced by the  $\text{H}_2$  radiative cascade. It is evident from the figure that distortion photons coming from primordial atomic recombination represent the main non-thermal contribution to the reaction rate.

For reaction (9) we have adopted the analytical fit of Tegmark et al. (1997) to the cross section data computed by Wishart (1979). In Figure 4 we show the  $\text{H}^-$  photodetachment rate coefficient obtained considering both the integration over the CMB and the distortion photons. The former clearly provides the largest contribution at redshifts greater than  $z \sim 100$ , whereas at lower redshift hydrogen recombination photons contribute significantly. The effect of helium photons is restricted to very early times ( $z \simeq 2400$ )

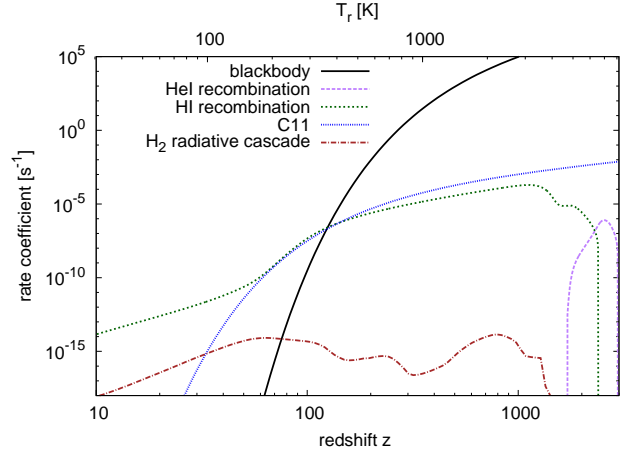


**Figure 4.**  $\text{H}^-$  photodetachment rate coefficient. Separate contribution of the blackbody spectrum, H and He recombination photons, and  $\text{H}_2$  radiative cascade are shown. As in the case of  $\text{H}_2^+$  photodissociation, atomic recombination represents the dominant non-thermal contribution.

when only very insignificant amounts of chemical elements have formed. The feedback of helium photons on hydrogen also creates extra features in the Ly- $\alpha$  recombination spectrum that leads to non-monotonic behavior of the  $\text{H}^-$  photodetachment rate at  $z \simeq 1800$ . It is also important that at high redshifts ( $z \simeq 1300$ ) half of the non-thermal reaction rate is caused by the 2s-1s continuum emission, while in the post-recombination epoch only the H I Ly- $\alpha$  distortion is important. As for  $\text{H}_2^+$  photodissociation, the process of  $\text{H}_2$  radiative cascade remains negligible at all redshifts.

### 3 REACTION RATES AND KINETICS

The chemistry of the early Universe at  $z < 10^3$  can be described as the kinetics of a H-He plasma in an expanding medium. For this reason, the following time-dependent system of ordinary differential equations (see, e.g. Galli & Palla 1998) has to be solved:

$$\begin{aligned} \frac{dN_i}{dt} = & - \sum_l \tilde{k}_l N_i - \sum_j k_{ij} N_i N_j + \\ & + \sum_n \tilde{k}_n N_n + \sum_j \sum_m \check{k}_i^{jm} N_j N_m, \end{aligned} \quad (10)$$

where  $N_i$  is the abundance of the  $i^{\text{th}}$  species relative to the total baryon density,  $\tilde{k}_l$  are the photodestruction rate coefficients of the  $i^{\text{th}}$  species via the  $l^{\text{th}}$  photoprocess;  $k_{ij}$  are the destruction rate coefficients for the  $i^{\text{th}}$  species for collisions with the  $j^{\text{th}}$  chemical partner;  $\tilde{k}_n$  are the formation rate coefficients of the  $i^{\text{th}}$  species due to the  $n^{\text{th}}$  photodestruction process for the  $N_n$  species and  $\check{k}_i^{jm}$  are the formation rate coefficients of the  $i^{\text{th}}$  species due to collisions between the  $j^{\text{th}}$  and  $m^{\text{th}}$  species. Each reaction rate is proportional to the variation of the baryonic density as a function of time

$$n_b(z) = \Omega_b \frac{3H_0^2}{8\pi G \mu m_H} (1+z)^3, \quad (11)$$

where  $\Omega_b$  is the baryon fraction,  $H_0 = 100h \text{ km s}^{-1} \text{ Mpc}^{-1}$  is the Hubble constant with  $h = 0.705$ ,  $G$  is the gravitational constant,  $m_H$  is the atomic hydrogen mass, and

$\mu = 4/(4 - 3Y_p)$  is the mean atomic weight of the gas,  $Y_p$  denoting the helium fractional abundance by mass. The equations for the radiation and gas temperatures are solved in order to evaluate the specific velocity of each chemical process in the kinetics. For the present calculations, the cosmological parameters from WMAP7 and standard BBN data have been used (Komatsu et al. 2011; Iocco 2012).

For our network, we adopted the rate coefficients summarized in Table B. The table also provides polynomial fits to the non-thermal contributions to the photodetachment of  $H^-$  and photodissociation of  $H_2^+$  rates. When applicable, the complete vibrational manifolds of  $H_2$  and its cation were used, both in LTE approximation in the entrance channel and as sum of contributions in the exit channel.

## 4 RESULTS

Using the new rates and the improved rate coefficients reported in C11, we determined the fractional abundances of several atomic and molecular species with the kinetic model described in the previous section. Figure 5 shows the evolution of  $H_2$ ,  $H_2^+$ ,  $H_3^+$  and HD, along with that of  $H^-$  and  $D^-$ . The main differences with respect to previous studies can be summarized as follows: starting at high redshifts, the abundances are affected by the enhanced  $H_2$  destruction channels ( $H_2/H^+$  charge transfer, dissociation via H and  $H^+$  collisions, photodestruction),  $H^-$  photodetachment and modified  $H/H^-$  associative detachment. The first process results in a reduced fractional abundance of  $H_2$  at redshifts  $z \sim 1000$ , where it reaches values roughly one order of magnitude smaller than in previous calculations (e.g. Schleicher et al. 2008). Consequently, the fractional abundances of HD and  $H_3^+$  are reduced in the same redshift range. This effect is caused by the inclusion of the entire vibrational manifold, as also found by Capitelli et al. (2007) for the dissociative attachment process of  $H_2$  (see Figures 4-6 of C11).

At lower redshifts, the abundances are affected by the combined effect of the enhanced photodetachment of  $H^-$  and the decrease of the efficiency of associative detachment due to non-thermal photons. This result qualitatively agrees with what was found in the steady-state model by Hirata & Padmanabhan (2006), where however no expression for the non-thermal rate coefficient was given, and here a more detailed treatment for the recombination spectrum is used. The effect of the contribution of non-thermal photons to the photodetachment of  $H^-$  can be appreciated in Figure 5 (bottom panel) at  $z < 100$ . Although the freeze-out value of  $H^-$  at low  $z$  remains unchanged, the abundance of  $H_2$  is reduced by about 70% at the epochs when the  $H^-$  channel is dominant. Importantly, the new evolution reduces the final rise of the  $H_2$  abundance at  $z \sim 100$  that characterized all previous calculations. It is also worth noting that, despite the huge effect of non-thermal photons on the photodissociation of  $H_2^+$ , its abundance is not significantly affected. This can be understood considering the relatively high threshold energy for the photodissociation process compared to the photodetachment of  $H^-$  and to the mean thermal energy available. Indeed, the integration over the high frequency part of the distortion spectrum is much more favourable for lower thresholds, as it can be derived from Fig. 1.

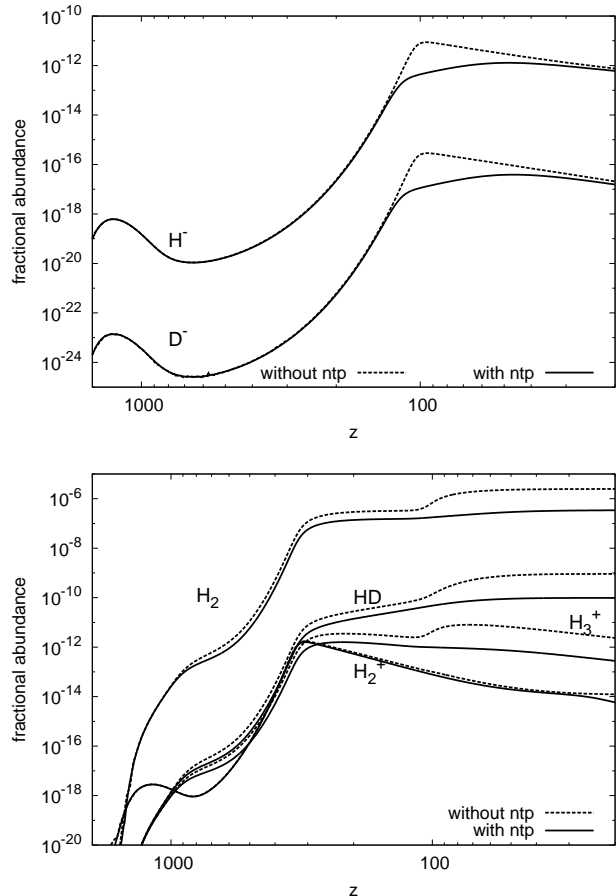


**Figure 5.** Fractional abundances of selected species:  $H_2$ , HD and  $H_3^+$  (top panel),  $H^-$  and  $D^-$  (bottom panel), with and without non-thermal photons (green dotted and blue solid curves, respectively.)

To compare the efficiency of each process included in the kinetic model, Figure 6 shows the destruction and formation rates for  $H_2$  as a function of  $z$ . It should be noted that the dissociation of  $H_2$  via  $H^+$  collisions (process labelled “6d” in the figure) is one of the most efficient destruction mechanisms, although it is usually neglected. For the formation channels, the effect of non-thermal photons is most evident in the channel of associative detachment (process “2f”).

## 5 CONCLUSIONS

We followed the formation and destruction of the main molecules and molecular ions in the early Universe, focusing on the effect of non-thermal photons produced by the recombination of H and He and by the non-equilibrium formation of  $H_2$ . We computed the changes in the fractional abundances of  $H_2$ ,  $H^-$ ,  $H_2^+$ ,  $H_3^+$  and on deuterated species such as  $D^-$  and HD. We find that because of high-energy tails in the photon spectra at several  $z$ , the efficiency of photodestruction is greatly enhanced, yielding lower fractional elemental abundances than in the standard thermal treatment of the chemical kinetics.

We also showed that the inclusion of vibrational lev-

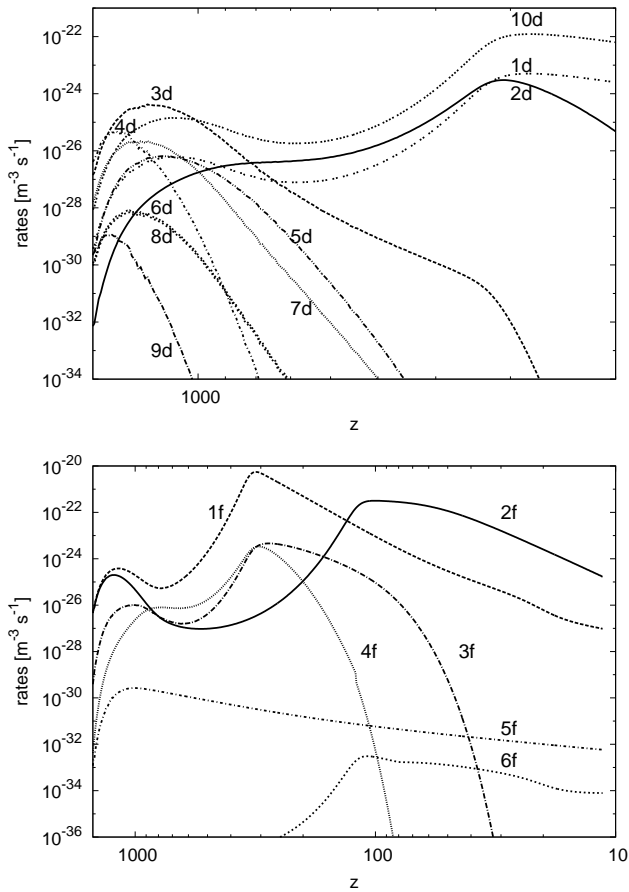


**Figure 6.**  $\text{H}_2$  destruction (*top panel*) and formation (*bottom panel*) rates as a function of redshift  $z$ . Destruction processes:  $\text{D}^+ + \text{H}_2 \rightarrow \text{HD} + \text{H}^+$  (1d);  $\text{D} + \text{H}_2 \rightarrow \text{HD} + \text{H}$  (2d);  $\text{H}^+ + \text{H}_2 \rightarrow \text{H}_2^+ + \text{H}$  (3d);  $\text{H}_2 + h\nu \rightarrow 2\text{H}$  (indirect, 4d);  $\text{H}_2 + \text{H} \rightarrow 3\text{H}$  (5d);  $\text{H}_2 + \text{H}^+ \rightarrow 2\text{H} + \text{H}^+$  (6d);  $\text{H}_2 + e \rightarrow \text{H} + \text{H}^-$  (7d);  $\text{H}_2 + e \rightarrow 2\text{H} + e$  (8d);  $\text{H}_2 + h\nu \rightarrow \text{H}_2^+ + e$  (9d);  $\text{H}^+ + \text{H}_2 \rightarrow \text{H}_3^+ + h\nu$  (10d). Formation processes:  $\text{H}_2^+ + \text{H} \rightarrow \text{H}_2 + \text{H}^+$  (1f);  $\text{H}^- + \text{H} \rightarrow \text{H}_2 + e$  (2f);  $\text{HD} + \text{H}^+ \rightarrow \text{D}^+ + \text{H}_2$  (3f);  $\text{HD} + \text{H} \rightarrow \text{D} + \text{H}_2$  (4f);  $2\text{H} + \text{H} \rightarrow \text{H}_2 + \text{H}$  (5f);  $\text{H}_2^+ + \text{H}^- \rightarrow \text{H} + \text{H}_2$  (6f).

els in the calculation of reaction rates is critical for their determination at high temperatures when excited levels are more populated. At high  $z$ , where these conditions apply, the resulting fractional abundances of  $\text{H}_2$  and  $\text{H}_2^+$  are reduced by a factor of  $\sim 10$ . However, if used in other environments where molecular hydrogen is more abundant (e.g. during the collapse of primordial clouds), these new rates are expected to affect more significantly the final molecular abundances.

## ACKNOWLEDGMENTS

The authors acknowledge the referee Steve Lepp for a careful reading of the paper. We are very grateful to Anatolij A. Mihajlov and Lj. M. Ignjatovic (Institute of Physics, University of Belgrade) for providing photodissociation cross section data computed over a wide range of wavelengths and temperatures. CMC and SL acknowledge financial support of MIUR-Università degli Studi di Bari, (“fondi di Ateneo 2010”) and MIUR-PRIN (grant no. 2010ERFKXL). JC was

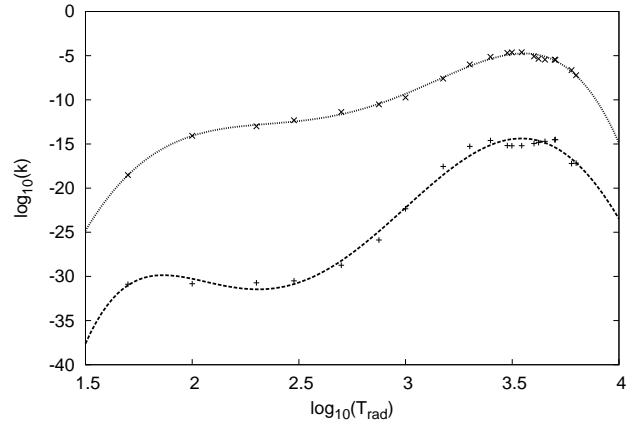


**Figure A1.** Fits (*dashed lines*) for the contribution of non-thermal photons to the photodissociation of  $\text{H}_2^+$ . *Upper curve*: primordial hydrogen recombination contribution; *lower curve*:  $\text{H}_2$  radiative cascade contribution.

supported by DoE SC-0008108 and NASA NNX12AE86G. This work has also been partially supported by the FP7 project “Phys4Entry” - grant agreement n. 242311.

## APPENDIX A: FITTING FORMULAE FOR THE RATE COEFFICIENTS

We fitted the reaction rate coefficients for the photodissociation of  $\text{H}_2^+$  and the photo detachment of  $\text{H}^-$  with logarithmic polynomials of the form

$$\log k(T_r) = \sum_n a_n (\log T_r)^n. \quad (\text{A1})$$

The coefficients of Eq. (A1) are given in Table B, together with the complete set of reaction rates employed in the kinetic model. The temperature of gas and radiation are indicated by  $T_g$  and  $T_r$ , respectively, and are expressed in K. Natural logarithms are indicated as  $\ln$ , logarithms to base 10 as  $\log$ . The results of the fitting formulae are compared to the numerical results in Figures A1-A2.

## APPENDIX B: DARK MATTER (DM) ANNIHILATION

Dark matter annihilation or decay leads to extra ionizations of hydrogen and helium atoms in the early Universe (Chen & Kamionkowski 2004; Padmanabhan & Finkbeiner 2005), delaying the cosmological recombination process (Peebles et al. 2000) and causing emission of extra recombination photons (Chluba 2010). The additional injection of energy and photons should be taken into account when considering the physical phenomena occurring in the primeval plasma as well as the chemistry. Here we evaluate the effect of extra photons produced by the direct reprocessing of annihilation energy by hydrogen on the rate coefficient of  $\text{H}^-$  photodetachment. Details on the equations employed and their derivation can be found in Chluba (2010).

The energy release associated with the annihilation of some DM particle  $\chi$  with its antiparticle  $\bar{\chi}$  depends on the

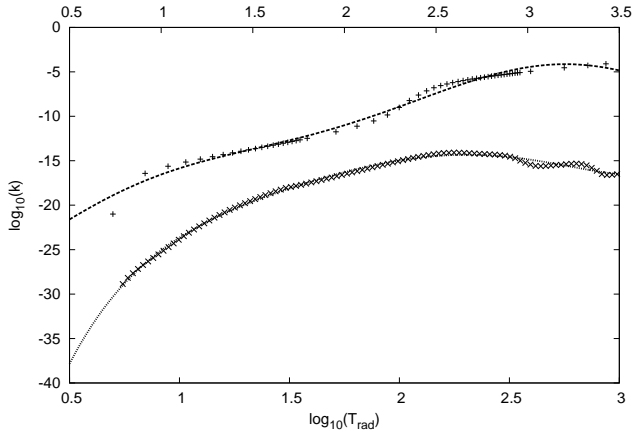


**Figure A2.** Fits (*dashed lines*) for the contribution of non-thermal photons to the photodetachment of  $\text{H}^-$ . *Upper curve and x-axis*: primordial hydrogen recombination contribution; *lower curve and x-axis*:  $\text{H}_2$  radiative cascade contribution. Their validity corresponds to the temperature ranges of each axis.

mass of the particles involved, on the fractional abundances of particle/antiparticle and on the thermally averaged cross section  $\langle\sigma v\rangle$  for that process:

$$\frac{dE}{dt} \sim M_\chi c^2 \langle\sigma v\rangle N_\chi N_{\bar{\chi}} \quad [\text{eV cm}^{-3} \text{ s}^{-1}] \quad (\text{B1})$$

Here, results are given as a function of the annihilating efficiency of the particle/antiparticle pair  $\epsilon_0$ :

$$\frac{dE_d}{dt} = \epsilon_0 N_{\text{H}}(z) (1+z)^3 \quad (\text{B2})$$

In Figure B1 we show the cases  $\epsilon_0 = 10^{-23}$ ,  $10^{-24}$  and  $5 \times 10^{-24} \text{ eV s}^{-1}$ . The presence of extra photons increases the  $\text{H}^-$  photodetachment rate considerably: the larger the annihilating efficiency the stronger the destruction process. In particular, in the range of annihilating efficiencies shown in the figure and for  $z < 70$ , the enhancement to the rate coefficient scales as:

$$f(\epsilon_0) \sim 1 + 0.44(\epsilon_0/10^{-24}) \quad (\text{B3})$$

This implies that the early Universe chemistry is not only sensitive to direct ionizations induced by the annihilation products, but also to the reprocessed energy causing additional ionizations of abundant neutral hydrogen atoms and reemission of Ly- $\alpha$  photons.

## REFERENCES

- Abel, T., Bryan, G. L., & Norman, M. L. 2002, *Science*, 295, 93
- Abel, T., Anninos, P., Zhang, Y., & Norman, M. L. 1997, *New Astron.*, 2, 181 (AAZN97)
- Argyros, J.D., 1974, *J. Phys. B*, 7, 2025
- Bovino, S., Tacconi, M., Gianturco, F. A., & Galli, D., 2011, *A&A*, 529, A140 (BTGG11)
- Bromm, V., Coppi, P. S., & Larson, R. B. 2002, *ApJ*, 564, 23
- Capitelli, M., Coppola, C. M., Diomedede, P., Longo, S., 2007, *A&A*, 470, 811 (CCDL07)

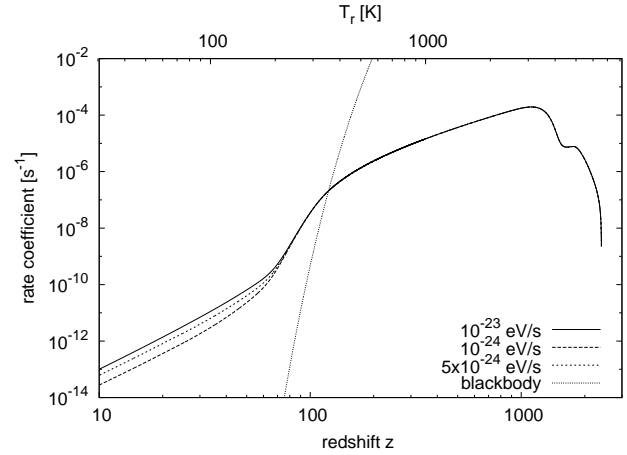


**Figure B1.**  $\text{H}^-$  photodetachment: effect of dark matter annihilation on the reaction rate. Calculations are reported for different annihilating efficiency, namely  $\epsilon_0 = 10^{-23} \text{ eV/s}$ ,  $10^{-24} \text{ eV/s}$ ,  $5 \times 10^{-24} \text{ eV/s}$ .

- Čížek, M., Horáček, J., Domcke, W., 1998, *J. Phys. B: Atom., Molec. & Opt. Phys.*, 31, 2571
- Chen, X., & Kamionkowski, M. 2004, *Phys.Rev.D*, 70, 043502
- Chluba, J., & Sunyaev, R. A. 2006, *A&A*, 458, L29
- Chluba, J., & Sunyaev, R. A. 2007, *A&A*, 475, 109
- Chluba, J., Sunyaev, R.A., 2008, *A&A*, 480, 3, 1629
- Chluba, J., & Sunyaev, R. A. 2010, *MNRAS*, 402, 1221
- Chluba, J., & Sunyaev, R. A. 2012, *MNRAS*, 419, 1294
- Chluba, J., 2010, *MNRAS*, 402, 1195
- Chluba, J., Rubiño-Martín, J. A., Sunyaev, R. A., 2007, *MNRAS*, 374, 4, 1310
- Chluba, J., & Thomas, R. M. 2011, *MNRAS*, 412, 748
- Ciardi, B., & Ferrara, A., 2001, *MNRAS*, 324, 648
- Coppola, C. M., Longo, S., Capitelli, M., Palla, F., Galli, D., 2011, *ApJS*, 193, 7 (C11)
- Coppola, C. M., D’Introno, R., Galli, D., Tennyson, J., Longo, S., 2012, *ApJS*, 199, 16
- Dalgarno, A., 2005, *J. of Phys., Conf. Ser.*, 4, 10
- Dickinson, A. S., 2008, *J. Phys. B: At. Mol. Opt. Phys.*, 41, 049801 (DI08)
- Dunn, G., 1968, *Phys. Rev.*, 172, 1
- Flower, D., 2000, *A&A*, 362, 774
- Fixsen, D. J., Cheng, E. S., Gales, J. M., et al. 1996, *ApJ*, 473, 576
- Fixsen, D. J. 2009, *ApJ*, 707, 916
- Galli, D., Palla, F., 1998, *A&A*, 335, 403 (GP98)
- Galli, D., Palla, F. 2002, *PSS*, 50, 1197 (GP02)
- Gong, Y., Cooray, A., Santos, M. G., *ApJ* accepted, arXiv:1212.2964
- Hirata, C. M., Padmanabhan, N., 2006, *MNRAS*, 372, 3, 1175
- Iocco, F., 2012, *Mem. S.A.It. Suppl.*, 22, 19
- Juřek, M., Špirko, V., Kraemer, W. P. 1995, *Chem. Phys.*, 193, 287 (JSK95)
- Komatsu, E., et al., 2011, *ApJS*, 192, 18
- Khatri, R., & Sunyaev, R. A., 2012, *Journal of Cosmology and Astroparticle Physics*, 6, 1
- Kreckel, H., Bruhns, H., Čížek, M., Glover, S. C. O., Miller, K. A., Urbain, X., Savin, D. W., 2010, *Sci.* 329, 69

**Table B1.** Reaction rates.

Process	Reaction rates [MKS]	Ref
1) $\text{H} + \text{e}^- \rightarrow \text{H}^- + h\nu$	$1.4 \times 10^{-24} T_{\text{g}}^{0.928} e^{-T_{\text{g}}/16200}$	GP98
2) $\text{H}^- + \text{e}^- \rightarrow \text{H} + 2\text{e}^-$	fit from reference	AAZN97
3) $\text{H}^- + \text{H} \rightarrow 2\text{H} + \text{e}^-$	fit from reference	AAZN97
4) $\text{H}^- + \text{H}^+ \rightarrow 2\text{H}$	$1.40 \times 10^{-13} (T_{\text{g}}/300)^{-0.487} e^{T_{\text{g}}/29300}$	LSD02
5) $\text{H}^- + h\nu \rightarrow \text{H} + \text{e}^-$		
thermal	$0.11 T_{\text{r}}^{2.13} e^{-8823/T_{\text{r}}}$	GP98
non-thermal: atom. recomb.	$\log k = \sum_{n=0}^6 a_n (\log T_{\text{r}})^n$ $a_0 = -26.6463$ $a_1 = 3.35998$ $a_2 = 25.729$ $a_3 = -31.6442$ $a_4 = 15.9545$ $a_5 = -3.60013$ $a_6 = 0.298272$	this work
non-thermal: $\text{H}_2$ radiative cascade	$\log k = \sum_{n=0}^5 b_n (\log T_{\text{r}})^n$ $b_0 = -81.12$ $b_1 = 139.379$ $b_2 = -137.531$ $b_3 = 73.0553$ $b_4 = -19.4282$ $b_5 = 1.99768$	this work
6) $\text{D}^- + h\nu \rightarrow \text{D} + \text{e}^-$	as fit for reaction (5)	S08
7) $\text{HD}^+ + h\nu \rightarrow \text{D} + \text{H}^+$	$(1/2) \times 1.63 \times 10^7 e^{-32400/T_{\text{r}}}$	S08
8) $\text{HD}^+ + h\nu \rightarrow \text{D}^+ + \text{H}$	$(1/2) \times 1.63 \times 10^7 e^{-32400/T_{\text{r}}}$	S08
9) $\text{HD}^+ + h\nu \rightarrow \text{H}^+ + \text{D}^+ + \text{e}^-$	$9.0 \times 10^1 T_{\text{r}}^{1.48} e^{-335000/T_{\text{r}}}$	S08
10) $\text{HD} + h\nu \rightarrow \text{HD}^+ + \text{e}^-$	$2.9 \times 10^2 T_{\text{r}}^{1.56} e^{-178500/T_{\text{r}}}$	S08
11) $\text{D} + \text{H}^+ \rightarrow \text{D}^+ + \text{H}$	$2.0 \times 10^{-16} T_{\text{g}}^{0.402} e^{-37.1/T_{\text{g}}} - 3.31 \times 10^{-23} T_{\text{g}}^{1.48}$	SA02
12) $\text{D}^+ + \text{H} \rightarrow \text{D} + \text{H}^+$	$2.06 \times 10^{-16} T_{\text{g}}^{0.396} e^{-33.0/T_{\text{g}}} + 2.03 \times 10^{-15} T_{\text{g}}^{-0.332}$	SA02
13) $\text{D} + \text{H} \rightarrow \text{HD} + h\nu$	$10^{-32} [2.259 - 0.6(T_{\text{g}}/10^3)^{0.5} + 0.101(T_{\text{g}}/10^3)^{-1.5} - 0.01535(T_{\text{g}}/10^3)^{-2} + 5.3 \times 10^{-5}(T_{\text{g}}/10^3)^{-3}]^{-3}$	DI08
14) $\text{HD}^+ + \text{H} \rightarrow \text{HD} + \text{H}^+$	$6.4 \times 10^{-16}$	SLD98
15) $\text{D} + \text{H}^+ \rightarrow \text{HD}^+ + h\nu$	$\log k/10^{-6} = -19.38 - 1.523 \log T_{\text{g}} + 1.118(\log T_{\text{g}})^2 - 0.1269(\log T_{\text{g}})^3$	GP98
16) $\text{D}^+ + \text{H} \rightarrow \text{HD}^+ + h\nu$	as fit for reaction (15)	GP98
17) $\text{HD}^+ + \text{e}^- \rightarrow \text{D} + \text{H}$	$7.2 \times 10^{-14} T_{\text{g}}^{-0.5}$	SLD98
18) $\text{D} + \text{e}^- \rightarrow \text{D}^- + h\nu$	$3.0 \times 10^{-22} (T_{\text{g}}/300)^{0.95} e^{-T_{\text{g}}/9320}$	SLD98
19) $\text{D}^+ + \text{D}^- \rightarrow 2\text{D}$	$1.96 \times 10^{-13} (T_{\text{g}}/300)^{-0.487} e^{T_{\text{g}}/29300}$	LSD02
20) $\text{H}^+ + \text{D}^- \rightarrow \text{D} + \text{H}$	$1.61 \times 10^{-13} (T_{\text{g}}/300)^{-0.487} e^{T_{\text{g}}/29300}$	LSD02
21) $\text{H}^- + \text{D} \rightarrow \text{H} + \text{D}^-$	$6.4 \times 10^{-15} (T_{\text{g}}/300)^{0.41}$	SLD98
22) $\text{D}^- + \text{H} \rightarrow \text{D} + \text{H}^-$	$6.4 \times 10^{-15} (T_{\text{g}}/300)^{0.41}$	SLD98
23) $\text{D}^- + \text{H} \rightarrow \text{HD} + \text{e}^-$	$1.5 \times 10^{-15} (T_{\text{g}}/300)^{-0.1}$	SLD98
24) $\text{D} + \text{H}^- \rightarrow \text{HD} + \text{e}^-$	as fit for reaction (22)	S08
25) $\text{H}^- + \text{D}^+ \rightarrow \text{D} + \text{H}$	$1.61 \times 10^{-13} (T_{\text{g}}/300)^{-0.487} e^{T_{\text{g}}/29300}$	LSD02
26) $\text{He} + \text{H}^+ \rightarrow \text{He}^+ + \text{H}$	$4.0 \times 10^{-43} T_{\text{g}}^{4.74}$ for $T_{\text{g}} > 10^4$ $1.26 \times 10^{-15} T_{\text{g}}^{-0.75} e^{-127500/T_{\text{g}}}$ for $T_{\text{g}} < 10^4$	S08
27) $\text{He}^+ + \text{H} \rightarrow \text{He} + \text{H}^+$	$1.25 \times 10^{-21} (T_{\text{g}}/300)^{0.25}$	ZDKL89
28) $\text{He} + \text{H}^+ \rightarrow \text{HeH}^+ + h\nu$	$8.0 \times 10^{-26} (T_{\text{g}}/300)^{-0.24} e^{-T_{\text{g}}/4000}$	SLD98
29) $\text{He} + \text{H}^+ + h\nu \rightarrow \text{HeH}^+ + h\nu$	$3.2 \times 10^{-26} T_{\text{g}}^{1.8} e^{-T_{\text{g}}/4000} (1 + 2 \times 10^{-4} T_{\text{r}}^{1.1}) (1 + 0.17 T_{\text{g}}^{2.04})^{-1}$	JSK95, ZSD98
30) $\text{He}^+ + \text{H} \rightarrow \text{HeH}^+ + h\nu$	$4.16 \times 10^{-22} T_{\text{g}}^{-0.37} e^{-T_{\text{g}}/87600}$	SLD98
31) $\text{He}^+ + \text{e}^- \rightarrow \text{He} + \text{H}$	$3.0 \times 10^{-14} (T_{\text{g}}/300)^{-0.47}$	SLD98
32) $\text{HeH}^+ + h\nu \rightarrow \text{He} + \text{H}^+$	$2.20 \times 10^2 e^{-22740/T_{\text{r}}}$	JSK95
33) $\text{HeH}^+ + h\nu \rightarrow \text{He}^+ + \text{H}$	$7.8 \times 10^3 T_{\text{r}}^{1.2} e^{-240000/T_{\text{r}}}$	GP98

Krstić, P. S., Schultz, D. R., 1999, J. Phys. B: Atom., Molec. & Opt. Phys., 32, 2415  
 Krstić, P. S., Schultz, D. R., Janev, R. K., 2002, Phys. Scripta, T96, 61  
 Krstić, P. S., 2002, Phys. Rev. A, 66, 042717(1)  
 Krstić, P. S., 2003, Phys. Rev. A, 66, 022708(1)  
 Krstić, P. S., 2005, Nucl. Instr. & Meth. in Phys. Res. B, 241, 58

Lebedev, V. S., Presnyakov, L. P., Sobel'man, I. I., 2000, Astr. Rep., 11, 5, 338  
 Lebedev, V. S., Presnyakov, L. P., Sobel'man, I. I., 2003, Physics-Uspekhi, 46, 5, 473  
 Lepp, S., Stancil, P. C., & Dalgarno, A. 2002, JPhB, 35R, 57 (LSD02)  
 Longo, S., Coppola, C. M., Galli, D., Palla, F., Capitelli, M., 2011, Rend. Fis. Acc. Lincei, 22, 119



Table B2. Reaction rates.

Process	Reaction rates [MKS]	Ref
34) $\text{H}^- + \text{H} \rightarrow \text{H}_2 + \text{e}^-$	$\log k = -14.4 - 0.15(\log T_g)^2 - 7.9 \times 10^{-3}(\log T_g)^4$	C11
35) $\text{H}^+ + \text{H} \rightarrow \text{H}_2^+ + h\nu$	$\log(k/10^{-6}) = -19.38 - 1.523 \log T_g + 1.118(\log T_g)^2 - 0.1269(\log T_g)^3$	GP98
36) $\text{H}_2^+ + \text{H} \rightarrow \text{H}_2 + \text{H}^+$	$6.4 \times 10^{-16}$	GP98
37) $2\text{H} + \text{H} \rightarrow \text{H}_2 + \text{H}$	$5.5 \times 10^{-35} T_g^{-1}$	PSS83
38) $\text{H}_2 + \text{H}^+ \rightarrow \text{H}_2^+ + \text{H}$	$\ln k = a_0 + a_1 T_g + a_2 T_g^{-1} + a_3 T_g^2$ $a_0 = -33.081$ $a_1 = 6.3173 \times 10^{-5}$ $a_2 = -2.3478 \times 10^4$ $a_3 = -1.8691 \times 10^{-9}$	C11
39) $\text{H}_2 + \text{e}^- \rightarrow 2\text{H} + \text{e}^-$	$1.91 \times 10^{-15} T_g^{0.136} e^{-53407.1/T_g}$	TT02
40) $\text{H}^- + \text{H}^+ \rightarrow \text{H}_2^+ + \text{e}^-$	$6.9 \times 10^{-15} T_g^{-0.35}$ for $T_g < 8000$ $9.6 \times 10^{-13} T_g^{-0.9}$ for $T_g > 8000$	GP98
41) $\text{H}_2^+ + \text{e}^- \rightarrow 2\text{H}$	$k = \sum_{n=0}^5 a_n T_g^n$ $a_0 = 4.2278 \times 10^{-14}$ $a_1 = -2.3088 \times 10^{-17}$ $a_2 = 7.3428 \times 10^{-21}$ $a_3 = -7.5474 \times 10^{-25}$ $a_4 = 3.3468 \times 10^{-29}$ $a_5 = -5.528 \times 10^{-34}$	C11
42) $\text{H}_2^+ + \text{H}^- \rightarrow \text{H} + \text{H}_2$	$5 \times 10^{-12} T_g^{-0.5}$ for $T_g < 100$	AAZN97
43) $\text{H}_2 + \text{e}^- \rightarrow \text{H} + \text{H}^-$	$3.67 \times 10^{-5} T_g^{-2.28} e^{-47172/T_g}$	CCDL07
44) $\text{H}_2^+ + h\nu \rightarrow \text{H} + \text{H}^+$ thermal	$1.63 \times 10^7 e^{-32400/T_r}$	GP98
non-thermal: atom. recomb.	$\log k = \sum_{n=0}^5 a_n (\log T_r)^n$ $a_0 = -257.413$ $a_1 = 294.406$ $a_2 = -93.7846$ $a_3 = -13.1607$ $a_4 = 11.3683$ $a_5 = -1.46734$	this work
non-thermal: $\text{H}_2$ radiative cascade	$\log k = \sum_{n=0}^5 b_n (\log T_r)^n$ $b_0 = -1084.08$ $b_1 = 1990.32$ $b_2 = -1447.42$ $b_3 = 503.994$ $b_4 = -83.6462$ $b_5 = 5.28898$	this work
45) $\text{H}_2 + h\nu \rightarrow \text{H}_2^+ + \text{e}^-$	$3.06587 \times 10^9 e^{-18948.1/T_r}$	C11
46) $\text{H}_2^+ + h\nu \rightarrow 2\text{H}^+ + \text{e}^-$	$9 \times 10^1 T_r^{1.48} e^{-335000/T_r}$	GP98
47) $\text{H}_2 + h\nu \rightarrow \text{H}_2^* \rightarrow 2\text{H}$	$\ln k = 17.555 + 7.2643 \times 10^{-6} T_r - 1.4194 \times 10^5 T_r^{-1}$	C11
48) $\text{H}_2 + \text{H} \rightarrow \text{H} + \text{H} + \text{H}$	$1.9535 \times 10^{-10} T_g^{-0.93267} e^{-49743/T_g}$	C11
49) $\text{D} + \text{H}_2 \rightarrow \text{HD} + \text{H}$	$1.69 \times 10^{-16} e^{-4680T_g + 198800/T_g^2}$ for $T_g > 200$ $9 \times 10^{-17} e^{-3876/T_g}$ for $T_g < 200$	GP02 GP98
50) $\text{D}^+ + \text{H}_2 \rightarrow \text{HD} + \text{H}^+$	$10^{-15} [0.417 + 0.846 \log T_g - 0.137(\log T_g)^2]$	GP02
51) $\text{HD} + \text{H} \rightarrow \text{D} + \text{H}_2$	$5.25 \times 10^{-17} e^{-4430/T_g + 173900/T_g^2}$ for $T_g > 200$ $3.2 \times 10^{-17} e^{-3624/T_g}$ for $T_g < 200$	GP02 GP98
52) $\text{HD} + \text{H}^+ \rightarrow \text{D}^+ + \text{H}_2$	$1.1 \times 10^{-15} e^{-488/T_g}$	GP02
53) $\text{He} + \text{H}_2^+ \rightarrow \text{HeH}^+ + \text{H}$	$3 \times 10^{-16} e^{-6717/T_g}$	GP98
54) $\text{HeH}^+ + \text{H} \rightarrow \text{He} + \text{H}_2^+$	$4.3489 \times 10^{-16} T_g^{0.110373} e^{-31.5396/T_g}$	BTGG11
55) $\text{H}^+ + \text{H}_2 \rightarrow \text{H}_3^+ + h\nu$	$10^{-18}$	GP98
56) $\text{H}_3^+ + \text{e}^- \rightarrow \text{H} + \text{H}_2$	$4.6 \times 10^{-12} T_g^{-0.65}$	GP98
57) $\text{H}_2^+ + \text{H} \rightarrow \text{H} + \text{H}^+ + \text{H}$	$\ln k = a_0 + a_1 T_g + a_2 T_g^{-1} + a_3 T_g^2$ $a_0 = -32.912$ $a_1 = 6.9498 \times 10^{-5}$ $a_2 = -3.3248 \times 10^4$ $a_3 = -4.08 \times 10^{-9}$	C11
58) $\text{H}_2 + \text{H}^+ \rightarrow \text{H} + \text{H} + \text{H}^+$	$\ln k = a_0 + a_1 T_g + a_2 T_g^{-1} + a_3 T_g^2$ $a_0 = -33.404$ $a_1 = 2.0148 \times 10^{-4}$ $a_2 = -5.2674 \times 10^4$ $a_3 = -1.0196 \times 10^{-8}$	C11

- Mihajlov, A. A., Ignjatović, Lj. M., Sakan, N. M., Dimitrijević, M. S., 2007, *A&A*, 469, 2, 749
- Motapon, O., Tamo, F. O. W., Urbain, X., Schneider, I. F. 2008, *Phys. Rev. A*, 77, 5
- Pagel, B. E., 1959, *MNRAS*, 119, 609
- Palla, F., Salpeter, E. E., & Stahler, S. W. 1983, *ApJ*, 271, 632 (PSS83)
- Padmanabhan, N., & Finkbeiner, D. P. 2005, *Phys.Rev.D*, 72, 023508
- Peebles, P. J. E., Seager, S., & Hu, W. 2000, *ApJL*, 539, L1
- Rubiño-Martín, J. A., Chluba, J. and Sunyaev, R. A., 2006, *MNRAS*, 371, 1939
- Rubiño-Martín, J. A., Chluba, J., & Sunyaev, R. A. 2008, *A&A*, 485, 377
- Savin, D. W. 2002, *ApJ*, 566, 599 (SA02)
- Schleicher, D. R. G., Galli, D., Palla, F., Camenzind, M., Klessen, R. S., Bartelmann, M., Glover, S. C. O., 2008, *A&A*, 490, 2, 521 (S08)
- Schlemmer, S., 2011, *Angew. Chem. Int. Ed.*, 50, 2214
- Stancil, P.C., 1994, *ApJ*, 430, 360
- Stancil, P. C., Lepp, S., & Dalgarno, A. 1998, *ApJ*, 509, 1 (SLD98)
- Sunyaev, R. A., & Chluba, J. 2009, *Astronomische Nachrichten*, 330, 657
- Takagi, H., 2002, *Phys. Scripta*, T96, 52
- Tegmark, M., Silk, J., Rees, M. J., et al. 1997, *ApJ*, 474, 1
- Trevisan, C. S., & Tennyson, J. 2002, *Plasma Phys. Controlled Fusion*, 44, 1263 (TT02)
- Wishart, A. W., 1979, *MNRAS*, 187, 59P
- Wolniewicz, L., Simbotin, I., Dalgarno, A., 1998, *ApJS*, 115, 293
- Zygelman, B., Dalgarno, A., Kimura, M., & Lane, N. F. 1989, *Phys. Rev. A*, 40, 2340 (ZDKL89)
- Zygelman, B., Stancil, P. C., & Dalgarno, A. 1998, *ApJ*, 508, 151 (ZSD98)